Observation of a quasimolecular ionization window in low-to-intermediate impact velocity collisions of He^+ ions with H_2 and He

M. A. Abdallah,[1,*] W. Wolff,[2,†] H. E. Wolf,[2] L. F. S. Coelho,[2] C. L. Cocke,[3,‡] and M. Stöckli[3]
[1]*Physics Division, Oak Ridge National Laboratory, Oak Ridge, Tennessee 37831-6377*
[2]*Instituto de Fisica, Universidade Federal do Rio de Janeiro, Rio de Janeiro, Brazil*
[3]*Physics Department, Kansas State University, Manhattan, Kansas 66506*
(Received 13 September 1999; published 15 June 2000)

The ionization of H_2, leading to H_2^+ recoil ions in nondissociative states, and the ionization of He by incident He^+ ions were investigated in the 0.25–1.23-a.u. impact velocity range employing electron and target recoil-ion momentum-imaging techniques. Similarities as well as differences were observed in the electron velocity distributions from H_2 and He targets. In both cases the data strongly suggest of the promotion of molecular orbitals formed between target and projectile within a rather well-defined projectile velocity window. In particular, the data support the promotion of the $2p\pi$ molecular orbital populated via rotational coupling. Outside this molecular promotion window, in particular at lower velocities, mechanisms of a different kind appear to dominate the ionization process, and electron momentum distributions are very dissimilar for He and H_2. Reduced projectile scattering cross sections, derived from measured target recoil-ion transverse momentum distributions, support these conclusions and point to the coexistence, at certain impact velocities, of different ionization mechanisms.

PACS number(s): 34.50.Fa, 39.30.+w

I. INTRODUCTION

Ionization and other inelastic processes in atomic collisions provide, from the theoretical point of view, an ideal testing ground to describe the fundamental problem of the evolution of a time-dependent multiparticle system. Besides this basic importance, they are relevant over a broad range of pure and applied fields of research, such as astrophysics and stellar structure and evolution, plasma physics and thermonuclear fusion, and the study of surfaces and materials [1].

It is well established that for very slow collisions ($V_P \ll V_0$, where V_P is the projectile velocity and V_0 a typical target electron orbital velocity), molecular effects play a major role in inelastic collisions. In this low-velocity regime, the nuclear motion is considerably slower than the electronic motion, which allows an electron to be shared temporarily by the target and the projectile nuclei, thereby forming a transient quasimolecular ion [2]. This picture holds true even for large projectile velocities when inner-shell electrons are the active ones, as was suggested by Fano and Lichten [3], provided that $V_P \ll V_0$ still holds. In this model, as the internuclear separation decreases, electrons are promoted to states of higher energy and eventually into the continuum along a promoted molecular orbital (MO). This model was successfully used in explaining the *L* inner-shell vacancy formation in collisions of Ar^+ with Ar [4] as well as numerous other cases. Although most of the studies based on the molecular promotion model focused on the processes of excitation and charge exchange [5–10], it was suggested by several authors [7–9,11] that ionization at slow collision velocities could be treated based on the molecular promotion model as well.

When V_P becomes comparable to V_0, the nature of the process of ionization is expected to be less molecular. The two Coulomb centers are to be included in any treatment of what has come to be known as the two-center effect [12–16]. In 1983, Olson [17] used the classical-trajectory Monte Carlo method (CTMC) to study ionization and electron capture in the H^+-H($1s$) collision system. He noted that a large fraction of the electrons emitted into the forward direction possessed velocities approximately equal to half the projectile velocity. In a classical picture those are electrons left ''stranded'' at a point (called the ''saddle point'') in velocity space where they are subject to forces opposite in direction and equal in magnitude to the velocity produced by the Coulomb fields of the charged projectile and the residual ionized target. While the two Coulomb centers are receding from each other, those electrons will be pushed to higher energies on the rising potential of the saddle point. Eventually this process will leave the electrons riding the ''saddle'' in the continuum, when the two Coulomb centers become infinitely separated. Olson [18] and Olson *et al.* [19] studied in more detail those electrons within the CTMC framework and referred to them as $V_P/2$ electrons. This mechanism received support from coupled-channel calculations by Winter and Lin [20], who found that the inclusion of a third center in their close-coupling calculations resulted in a large improvement of the calculated cross section when compared to early experimental results by Fite *et al.* [21].

More recently, the ''saddle-point'' process received an alternative formulation in terms of the ''hidden-crossing'' theory [22–26]. In this theory two major mechanisms leading to ionization are identified, called the *T* and the *S* process, respectively. In both processes the electron is promoted to the continuum via successive ''hidden'' crossings of MOs formed during the collision. The term ''hidden'' refers to the

*Electronic address: abdallah@mail.phy.ornl.gov
†Electronic address: wania@if.ufrj.br
‡Electronic address: cocke@phys.ksu.edu

fact that these crossings take place in the complex plane of internuclear distances. In the *T* process electrons are promoted to the continuum while the two Coulomb centers are receding from each other; this process is the quantum-mechanical equivalent to the classical ''saddle-point'' mechanism. In the *S* process, on the other hand, an electron is ionized in a kind of adiabatic compression while the target and the projectile are approaching each other. While the two centers are approaching, a centrifugal barrier is formed between them, inside which electrons are excluded. Consequently, an electron may be pushed into the continuum while the target and the projectile are on their way to becoming a united atom (the point at which the barrier rises to infinity) [27]. It was demonstrated by Ovchinnikov and Macek [23] that this process leads to electron distributions in the continuum centered on both the target and the projectile. Since a considerable amount of theoretical support for the *T* process was provided by adiabatic calculations, which are expected to apply at much lower projectile velocities than those of most previous experimental investigations, Pieksma *et al.* [28] studied the velocity distribution of the electrons emitted from the collision system *p*-H in the projectile energy range 1–6 keV, where adiabatic theories do apply. Their data show an apparent dominance of the saddle-point ionization mechanism for energies ranging from 4 to 6 keV.

Experimentally, a great deal of work has been dedicated to searching for evidence for ''saddle-point'' electrons, with ambiguous results. An electron distribution centered on the saddle point is expected to shift with changing projectile charge and velocity according to

$$\vec{V}_s = \frac{\vec{V}_P}{1 + q_p^{1/2}/q_t^{1/2}}, \tag{1}$$

where $\vec{V}_P$ and $\vec{V}_s$ are the projectile and saddle-point velocities, and q_t and q_p are the target and projectile charges, respectively. The first experimental investigation of this mechanism was carried out by Olson *et al.* [19] by studying ionization during the collision *p*-He within a projectile energy range of 60–200 keV. A broad peak observed in the electron velocity spectrum at an angle of observation of 17° was considered as evidence for the existence of a saddle-point ionization mechanism. Most of the subsequent work focused on studying that peak [29–34]. In order to answer the question whether the electron longitudinal velocity distribution (i.e., velocity parallel to the incident projectile beam) does follow Eq. (1), Kravis *et al.* [35] and Abdallah *et al.* [36] performed a series of experiments with light, bare ions colliding with He and Ne. It was concluded that the maximum of the electron distributions did not follow the velocity and charge state dependence predicted by Eq. (1).

The entire field of ionization at low to intermediate ($V_P \leqslant 1.0$ a.u.) projectile velocities and the discussion of the saddle-point ionization mechanism was completely refocused by the striking and unexpected experimental results of Dörner *et al.* [37]. These authors applied the technique of cold target recoil-ion momentum spectroscopy (COLTRIMS) [38,39] to obtain a much more detailed, highly differential picture of the velocity distributions of electrons emitted in collisions of protons with He at projectile velocities of 0.45, 0.64, and 0.78 a.u. By measuring the three components of the target recoil-ion momentum, in addition to two velocity components of the ejected electron, they were able to determine electron velocity distributions for well-defined scattering planes and impact-parameter windows. They observed that electrons were ejected preferentially within the scattering plane and into the forward direction. The electrons exhibited a remarkable in-plane velocity distribution in the form of two''jets'' emanating from the target and separated by a valley along the projectile beam axis. These features were interpreted by Ovchinnikov and Macek [23] and Macek and Ovchinnikov [40,41]. The major idea is that one (or more) molecular orbital(s) is promoted into the continuum, carrying with it the character of that promoted orbital. This character is then revealed in the form of the continuum velocity distribution. Orbitals of various character have been implied by distributions such as those observed by Dörner *et al.* and in subsequent investigations carried out by our group. In the *p*-He case the dominant molecular orbital involved is identified as the promoted $2p\pi$ MO, and electron promotion into the continuum takes place via rotational coupling.

Using a similar COLTRIMS setup described below our group has investigated additional systems of $He^{+,2+}$ incident on He, Ne^+-Ne, He^+-Ne, and Ne^+-He at projectile velocities ranging from 0.25 to 1.23 a.u. [42–44]. Those studies have demonstrated that each collision system produces its own distinct electron velocity distribution. They served to re-enforce the concept of ionization in that particular impact velocity range proceeding via promoted molecular orbitals specific to each system.

In the present contribution we report on a detailed and comparative investigation of the ionization process in the collision systems He^+-He and He^+-H_2. From electron velocity as well as target recoil-ion momentum distributions, different ionization mechanisms have been identified, of molecular as well as nonmolecular nature, depending on the projectile velocity.

II. EXPERIMENTAL SETUP

The experiments were performed with the COLTRIMS setup installed at the J.R. Macdonald Laboratory CRYEBIS ion source facility [45] of Kansas State University. The targets consisted of cold supersonic gas jets of He and H_2 perpendicularly intersected by the projectile ion beam. A schematic drawing, not to scale, of the experimental setup is shown in Fig. 1(a). The electron-target recoil-ion spectrometer consisted of two position-sensitive detectors (2D-PSD) and a highly homogeneous electric extraction field. The field was directed perpendicular to both the incident projectile beam axis and the supersonic target jet. The detector planes were oriented parallel to the plane formed by the beam axis and the axis of the target jet [Fig. 1(b)].

A conventional coordinate system, to be used in the following presentation and discussion of results, is shown in Fig. 1(b). The projectile ion beam defines the *Z* axis, the *Y*

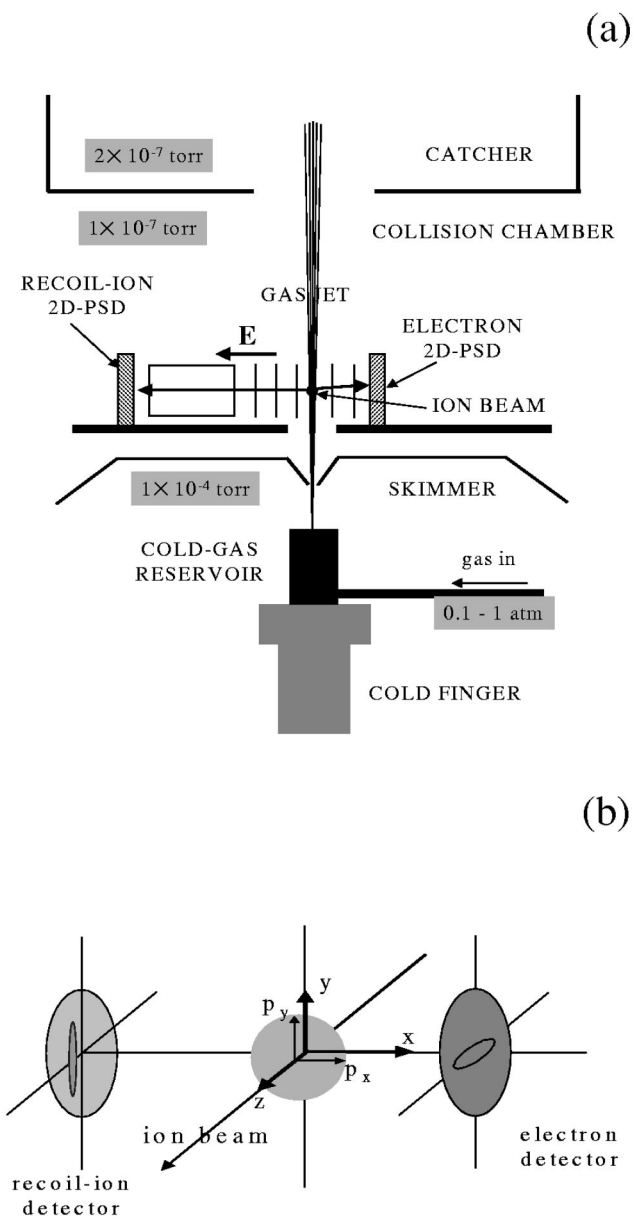

FIG. 1. (a) Schematic representation of the COLTRIMS setup used in this work. The projectile ion beam traverses the plane of the figure perpendicularly from back to front. The figure is not drawn to scale. (b) The coordinate system adopted for data reduction and analysis throughout the manuscript. Note that the planes of the position-sensitive detectors (2D-PSDs) are parallel to the YZ plane.

axis is chosen to coincide with the direction of the target gas jet, and the X axis is given by the direction of the electric extraction field. Two components of the recoil ion momentum vector $\vec{P}_r$ (P_{rY} and P_{rZ}) were reconstructed from the position of impact of the recoil-ion on the recoil detector. In the same way, two components of the electron velocity vector $\vec{V}_e$ (V_{eY} and V_{eZ}) were reconstructed from the position of impact of the electron on the electron detector. The third component of the recoil momentum vector, P_{rX}, was reconstructed from its flight time, with the time signal of the associated electron serving as a start signal to measure the recoil-ion flight time. This procedure introduces only a small amount of timing uncertainty, since the spread in electron flight time is much less than that in recoil-ion flight time.

The recoil-ion detector was calibrated in P_{rY} and P_{rZ} by performing a state-selective Ne^{10+}-He electron-capture experiment with known results [46,47], while the electron-detector was calibrated in part by performing ion-optical calculations. The origin of the coordinate system of the electron detector (zero point, $V_{eY}=V_{eZ}=0$) was determined experimentally by inverting the polarization of the electric extraction field, thereby accelerating recoil ions toward the electron detector. Since initial recoil momenta are small, the interaction region is located close to the electron detector, and a high extraction field was used, target recoil ions travel essentially along the X axis, regardless of their initial momentum. Their position of impact therefore provides the zero-point position of the electron detector. The position of the projectile beam axis ($V_{eY}=0$) on the electron detector was determined from ''side view'' electron velocity distributions as set forth in the section about electron ''side view'' distributions.

The resolution achieved in electron velocity distributions is limited by the width of the projectile beam (1 mm) in the Y direction, the width of the target gas jet (3.5 mm) in the Z direction, and the lack of a direct measurement of the electron flight time. The resolution in position of the electron detector itself (intrinsic resolution) was determined as 0.35 mm. The resolution in V_{eY}, limited by the finite beam size, depends on the strength of the applied extraction field (60–210 V/cm in the present case) and varies between 0.043 and 0.08 a.u. The resolution in V_{eZ} varied according to the extraction field between approximately 0.15 and 0.27 a.u. The recoil-ion detector had an intrinsic position resolution close to that of the electron detector. As was the case for the electron detector, the actual resolution depended on the electric extraction field applied. In the present case, where relatively strong fields had to be used, that resolution varied between 0.36 and 0.67 a.u.

III. DATA REDUCTION

The P_{rZ} component of the target recoil-ion momentum (also called the longitudinal recoil-ion momentum) provides information concerning the Q value of the ionizing collision via

$$Q \cong -V_P(P_{rZ}+P_{eZ}), \tag{2}$$

where Q is the electronic energy release. The transverse components of the recoil-ion momentum, P_{rX} and P_{rY}, were used to calculate the modulus of the transverse momentum:

$$P_{r\perp}=(P_{rX}^2+P_{rY}^2)^{1/2}. \tag{3}$$

The transverse momentum vector $\vec{P}_{r\perp}$ of the recoil ions balances, to a very good precision, the transverse momentum vector of the projectile ions after the collision. This is true since the transverse momentum of the ejected electrons, being of the order of or less than 0.2 a.u. in the projectile velocity range studied here, is in general much smaller than

that of the recoil ions. It follows that the laboratory scattering angle θ of the projectiles can be calculated from the recoil-ion transverse momentum $P_{r\perp}$ according to (P_0 stands for the initial projectile momentum)

$$\theta = P_{r\perp}/P_0. \tag{4}$$

One of the advantages of detecting electrons and associated target recoil ions in coincidence consists of the fact that the experiment allows for the selection of scattering planes. A scattering plane is defined by the momentum vector $\vec{P}_0$ of the incident projectile and the transverse momentum vector $\vec{P}_{r\perp}$ of the recoil ion. Two scattering planes are of particular interest: the plane parallel to the detector planes and the plane perpendicular to the detector planes. The first one is selected by choosing recoil ions with $P_{rX} \cong 0$, while the second one is characterized by recoil ions with $P_{rY} \cong 0$. Since electrons are detected in coincidence with target recoil ions, selecting only recoil ions with $P_{rX} \cong 0$ results in the generation of two-dimensional (V_{eY},V_{eZ}) electron velocity distributions that are projections of the three-dimensional (3D) distribution of the electron velocity vector onto the scattering plane. These distributions are called ''top views'' or in-plane distributions. On the other hand, the condition $P_{rY} \cong 0$ selects a scattering plane that cuts the electron detector perpendicularly. In this case the (V_{eY}, V_{eZ}) electron velocity distributions correspond to an edge view of the scattering plane and are therefore called ''side views.'' This kind of distribution reveals the degree of out-of-plane electron scattering. Note that, since the third electron velocity component V_{eX} is not measured, ''top view'' distributions give a complete picture of the 3D electron velocity distribution only if little out-of-plane scattering is present. The placement of representative top view and side view gates on a generic recoil-ion transverse momentum distribution is schematically indicated in Fig. 2(a).

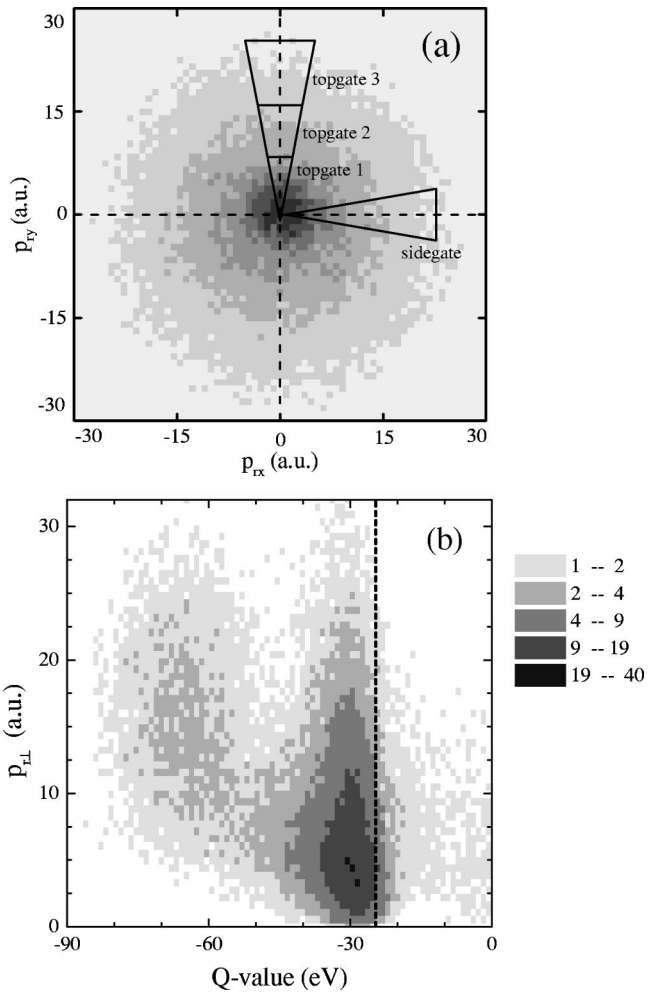

FIG. 2. Schematic of the placement of ''top view'' and ''side view'' gates on a generic recoil-ion transverse momentum distribution. (b) Q value dependence of the recoil-ion transverse momentum ($P_{r\perp}$) distribution for He^+-He at $V_P = 0.45$ a.u. Single target ionization and simultaneous ionization and excitation appear well separated in this figure. Simultaneous ionization and excitation is seen to occur at larger transverse recoil-ion momentum values (smaller impact parameters) than single target ionization. The dashed line indicates the position of the first ionization potential of helium.

IV. RESULTS

A. Recoil-ion momentum distributions

For molecular hydrogen targets, only the nondissociative ionization channel $He^+ + H_2 \rightarrow He^+ + H_2^+ + e$, which leaves the H_2^+ molecular recoil ion in a nondissociative state, was investigated. Figure 2(b) shows the relation between the recoil-ion transverse momentum $P_{r\perp}$ and its longitudinal momentum P_{rZ}, the latter one transformed into Q values according to Eq. (2), for He^+-He at 0.45 a.u. Two branches, corresponding to single target ionization and to simultaneous ionization and excitation, respectively, are visible. Projectile angular scattering cross sections can be generated from this type of distribution by projecting the respective branch onto the $P_{r\perp}$ axis. All subsequent data analysis has been performed for target single ionization only by placing a gate on the single ionization component.

Reduced projectile angular scattering cross sections corresponding to single target ionization were produced from distributions such as that of Fig. 2(b) for all projectile velocities as functions of the reduced scattering angle τ ($=E\theta$) and are shown in Figs. 3(a) and 3(b) for He^+-H_2 and He^+-He, respectively. The parameter τ is, for small scattering angles, a unique function of the impact parameter b, independent of beam energy, if a single classical internuclear scattering potential operates. The top scale shown in Fig. 3(b) is a calculated translation of τ to b for the interaction potential of two ground state He^+ ions, each assumed to maintain a static charge distribution throughout the collision. This is a model to allow an approximate association of τ and b. No such translation was attempted for the H_2 target, for which the scattering angle depends on the molecular alignment.

The cross sections in Fig. 3 are arbitrarily scaled, so that the curves corresponding to different projectile velocities, given in atomic units, are well separated. In the He^+-H_2 case the reduced cross-section curves for $V_P = 0.25 - 0.64$ a.u. are

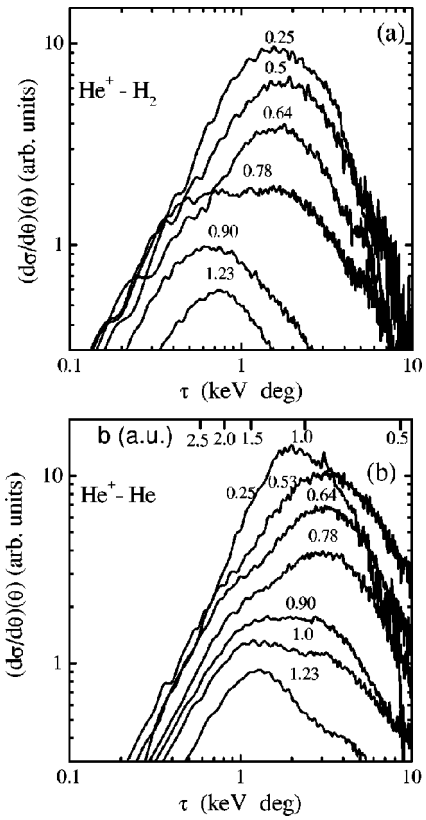

FIG. 3. Reduced projectile scattering cross sections as functions of the reduced scattering angle τ for He^+-H_2 (a) and He^+-He (b) generated from distributions such as that of Fig. 2(b) as described in the text. The curves are arbitrarily scaled to achieve separation. The numbers attached to the curves give the corresponding projectile velocity in atomic units. An impact parameter scale is shown for the He case (see text).

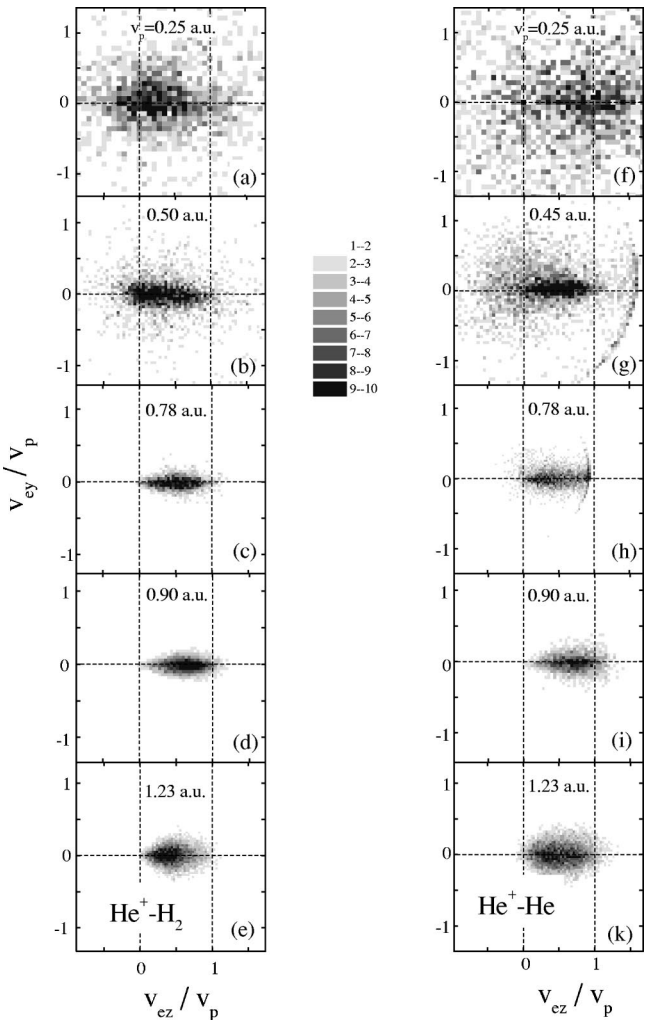

FIG. 4. ''Side view'' electron velocity (V_{eY}, V_{eZ}) distributions for (a)–(e) He^+-H_2 (left-hand column of figures) and (f)–(k) He^+-He (right-hand column of figures). The electron velocity components are given in units of the projectile velocity V_P, which is given in atomic units. The corresponding projectile velocity is indicated for each figure. The dashed lines mark the projectile beam ''position'' ($V_{eY}=0$) and the target ($V_{eZ}=0$) and projectile ($V_{eZ}=V_P$) ''positions'' in velocity space. Note that in (g) and (h) part of the edge of the electron detector appears in the form of a circular segment to the right of the electron velocity distribution. The intensity of each cell is proportional to the number of counts in that cell, as is indicated by the density scale. Each image has been normalized so its maximum intensity is near ten units on this scale.

basically identical in shape and position, with a maximum located between 1.6 and 1.7 keV deg. We will refer to this velocity region as the ''molecular window'' region, as discussed later. A similar value of 1.5 keV deg was observed by Dowek *et al.* [48] in He^+-H_2 collisions leading to direct target excitation ($n>2$), including ionization at a projectile energy of 1.0 keV. At 0.78 a.u., the corresponding cross-section curve suddenly broadens and appears to be composed of two maxima of about equal intensity, one located at about 0.7 and one at about 1.6 keV deg. At still higher projectile velocities, the maximum located at 1.6 keV deg has disappeared, and the cross sections are composed of a single maximum only, at about 0.7 keV deg. The He^+-He system, Fig. 3(b), exhibits a similar behavior. A shift in the position of the maximum, from 2 to 3 keV deg, is noted when passing from $V_P=0.25$ to 0.53 a.u. At larger projectile velocities, in the ''molecular window'' region, a second maximum, at about 1.2 keV deg, begins to emerge. At $V_P=0.9$ a.u. both maxima appear to be of about equal intensities. In fact, this curve has the same qualitative characteristics as the $V_P=0.78$ a.u. cross-section curve for He^+-H_2. At the two higher projectile velocities of 1.0 and 1.23 a.u., the maximum located at the larger reduced scattering angle of 3 keV deg rapidly yields to a new maximum at a smaller value of τ, as in the case of He^+-H_2.

B. Electron velocity distributions

We begin our presentation of electron velocity (V_{eY}, V_{eZ}) distributions with ''side views,'' which reveal the degree of out-of-plane electron scattering. Figure 4 shows side views for different projectile velocities, from 0.25 to 1.23 a.u. The left column of figures, 4(a)–4(e) refers to the He^+-H_2 collision system, while the right column, 4(f)–4(k), refers to He^+-He. In these figures the horizontal dashed line,

parallel to the V_{eZ} axis, indicates the projectile beam position ($V_{eY}=0$), while the two vertical dashed lines, parallel to the V_{eY} axis, mark the target ($V_{eZ}=0$) and projectile ($V_{eZ}=V_P$) position in velocity space. Both horizontal and vertical axes are given in units of V_P; the respective value of V_P is given in atomic units on each graph. In this and all subsequent figures showing density plots, a quantitative (relative) linear scale is given. Each image is presented on this same scale, with only the normalization of each image adjusted so that the maximum intensity is approximately ten units (proportional to the number of counts in that cell).

A substantial amount of out-of-plane electron scattering is noted at both the lowest and highest projectile velocities, while at intermediate velocities the electron distributions appear highly concentrated along the projectile beam axis, indicating that in-plane electron scattering dominates at these velocities. At $V_P=0.25$ a.u., the electrons appear widely dispersed over the detector area. This picture changes dramatically as V_P is raised to 0.50/0.45 a.u., at which point the target electrons begin to form a narrow ridge along the beam axis, with much less out-of-plane scattering. A low-intensity feature (''halo'') consisting of widely scattered out-of-plane electrons is noted for the He target. In addition, the ''halo'' exhibits a considerable amount of backward scattering ($V_{eZ}<0$). This feature is completely absent in the H_2 case. At the next two projectile velocities of 0.78 and 0.90 a.u. the ridge persists with very little out-of-plane electron scattering observed. The two side view distributions become wide again at the highest projectile velocity of 1.23 a.u. This behavior suggests that the confinement of the electrons to the collision plane is a characteristic of the molecular window region noted in the preceding section.

We now turn to ''top view'' electron velocity (V_{eY}, V_{eZ}) distributions, which represent the projection of the 3D electron velocity distribution onto the scattering plane. Several top views are shown for each projectile velocity. These correspond to different selections of the magnitude of the recoil-ion transverse momentum (P_{rX}, P_{rY}) as is shown schematically as top gates 1,2, and 3 in Fig. 2. The dashed lines in the various top view distributions have the same meaning as those in the side view distributions. In all top views the target recoil ion travels downward along the $V_{eZ}=0$ line.

We begin our discussion with the lowest projectile velocity of 0.25 a.u., Figs. 5(a) and 5(b), where a considerable amount of out-of-plane scattering has been observed in side views in the preceding paragraph. Similarities between top view and side view distributions are noted. In the H_2 target case, the top view electron distribution, Fig. 5(a), almost circular in shape, is strongly concentrated in the vicinity of $V_{eY}=V_{eZ}=0$, the target position, while in the He target case, Fig. 5(b), electrons are widely dispersed. However, a certain amount of asymmetry of the distribution, favoring the upper half ($V_{eY}>0$) of the scattering plane, is noted. One is not yet into the molecular window at this velocity.

At the next higher projectile velocity, near 0.5 a.u., one begins to enter the molecular window region [Figs. 5(c)–5(f)]. The electron distributions begin to concentrate along the projectile beam axis. The ''halo'' feature previously noted in side views for the He target appears in the form of a

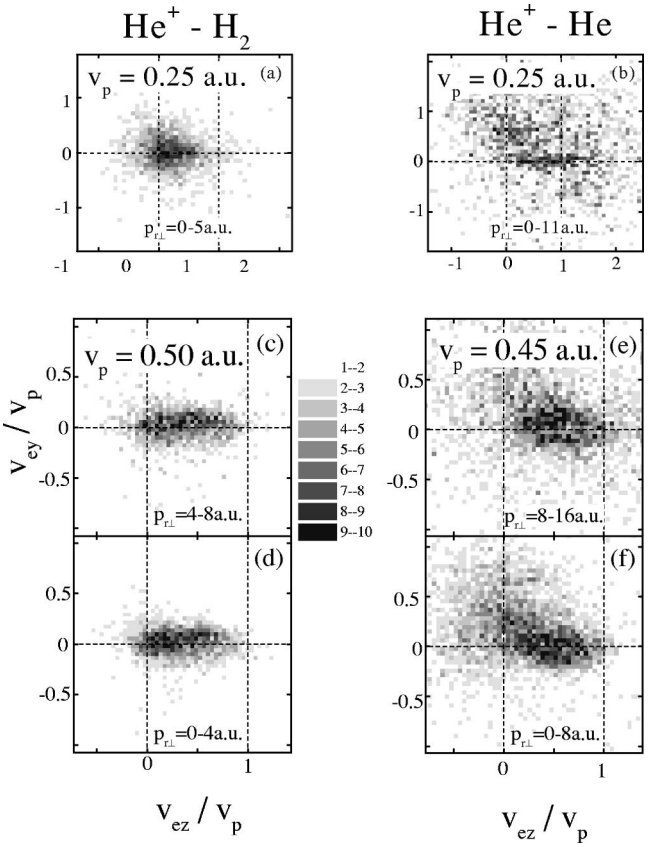

FIG. 5. ''Top view'' electron velocity distributions for projectile velocities of 0.25 a.u. (a) and (b) and near 0.5 a.u. (c)–(f), respectively. Figures (a) (c), and (d) refer to He^+-H_2, while (b), (e), and (f) refer to He^+-He. Axis units and the meaning of the dashed lines are the same as in Fig. 4. The target recoil ion travels downward.

low-intensity electron cloud asymmetrically placed in the upper half ($V_{eY}>0$) of the scattering plane and exhibiting a considerable degree of backscattering. The halo gradually tends to disappear with increasing projectile velocity, but persists up to 0.78 a.u. It is conspicuously absent in the H_2 case. As the beam velocity is raised from 0.5 to 0.64 a.u. and above (Figs. 6–8), the concentration of electrons along the projectile axis splits into two arched branches located off the beam axis and separated by a valley along the beam axis. This structure is visible for both targets. The electron intensity distribution along these branches is not constant, but varies with the projectile velocity. These branches become increasingly more arched with increasing recoil transverse momentum (decreasing impact parameter).

Finally, at the highest impact velocity of the present investigation of 1.23 a.u. (Fig. 9), the branches begin to break up (notably in the He case) and to form off-beam axis ''blobs,'' one located in the vicinity of the target and the other in the vicinity of the projectile.

C. Discussion and interpretation

For velocities between approximately 0.50 and 0.90 a.u., for both targets, the systematics of the electron distributions (appearance of geometrical patterns in the form of arched branches at larger target recoil momenta) are suggestive of a

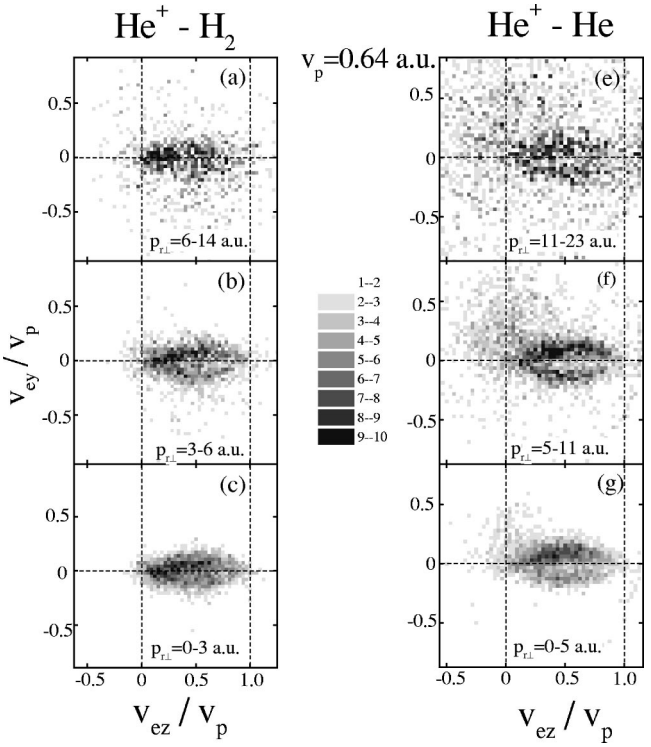

FIG. 6. ''Top view'' electron velocity distributions for He^+-H_2 [left-hand column, (a)–(c)] and He^+-He [right-hand column, (d)–(f)] at $V_P = 0.64$ a.u.

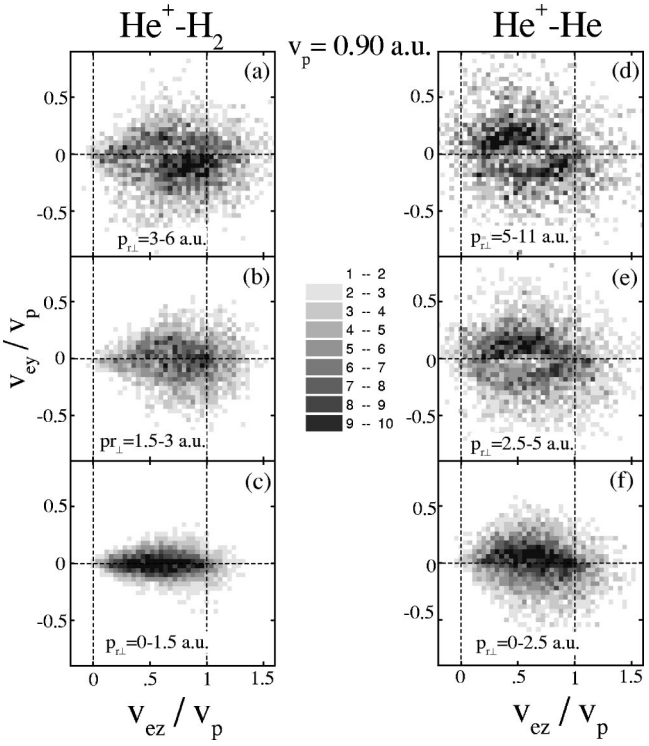

FIG. 8. The same as Fig. 6, but corresponding to a projectile velocity of 0.90 a.u.

molecular promotion mechanism. Where the projectile scattering cross sections of Fig. 3 suggest the coexistence of two distinct ionization mechanisms (for example, for velocities of 0.78 and above 0.9 a.u. for He and H_2, respectively), we attribute the larger angle feature to the molecular process. We are led to this interpretation by the fact that the geometrical patterns in the electron distributions are predominately confined to larger target recoil momenta, i.e. larger projectile scattering angles and consequently larger τ values .

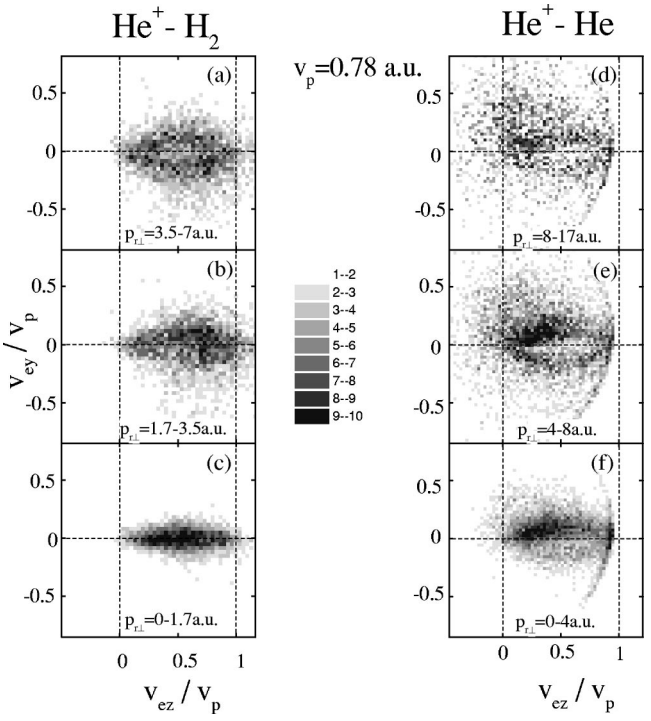

FIG. 7. The same as Fig. 6, but corresponding to a projectile velocity of 0.78 a.u.

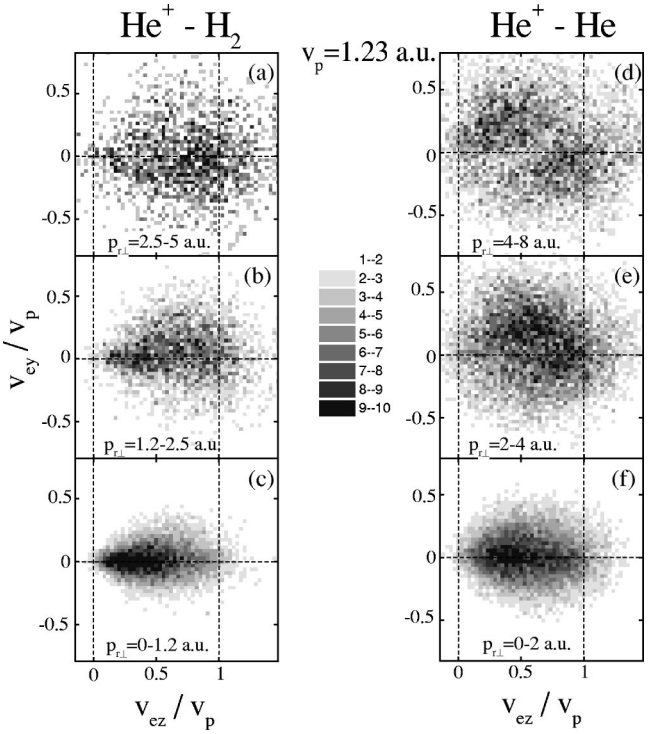

FIG. 9. The same as Fig. 6, but referring to $V_P = 1.23$ a.u.

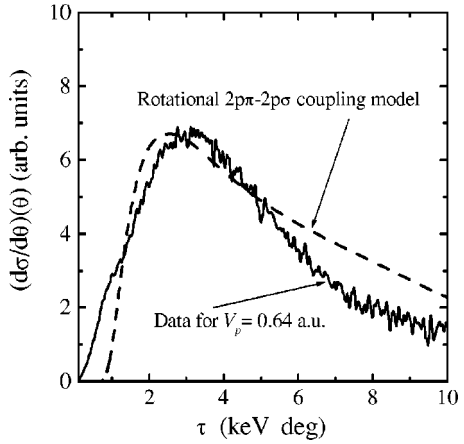

FIG. 10. Dashed line: calculated dependence of the population of the $2p\pi$ state, through rotational coupling with the $2p\sigma$ state, as a function of τ. Solid line: experimental data from Fig. 3 for a projectile velocity of 0.64 a.u. The vertical scale for the model has been adjusted to match that of the data.

It has been previously suggested [37,40,41] that the pattern of double branches, separated by a nodal line, arises from target ionization along a promoted $2p\pi$ molecular orbital. The process begins with a rotational coupling of the $2p\sigma$ orbital occupied by the incoming active electron into a $2p\pi$ one at small internuclear distances. The $2p\pi$ orbital is then eventually promoted via a series of radial crossings (the so-called *T* process) into the continuum. This process conserves the π character of the orbital and gives rise to the nodal line along the internuclear axis. The concentration of the electron distributions in the scattering plane is a natural result of such a mechanism, since only the $2p\pi$ orbital lying in the scattering plane is rotationally coupled. The unequal populations above and below the nodal line are attributed to a smaller but interfering σ amplitude whose phase relative to that of the π amplitude depends on both the beam velocity and the collision system. If the above mechanism holds, the impact-parameter (*b*) dependence of the process should be dominated by the enabling rotational coupling process, which transforms the $2p\sigma$ initial orbital into the $2p\pi$ one. The following promotion of the $2p\pi$ orbital into the continuum should subsequently occur at large *b* on the way out of the collision, and no strong *b* dependence is expected in this second step. We can test this conjecture for the case of He^+ on He by using the prescription given by Taulbjerg *et al.* [49] for the *b* dependence of the $2p\pi$-$2p\sigma$ rotational coupling process. We have used the energy-level curves shown in [7] to extract the value of ''alpha'' characterizing the separation of the orbitals as a function of internuclear distance. We then translated the calculated *b* dependence into a dependence on τ using a classical potential for the interaction of two frozen He^+ charge state distributions. The result is shown in Fig. 10 and compared to the experimental τ dependences of Fig. 3 for $V_P = 0.64$ a.u. In view of the simplicity of the model, we must interpret the agreement as supporting the argument that this rotational coupling mechanism enables the ionization process in the intermediate velocity range.

The strong similarity of the electron velocity distributions observed within the 0.5–0.9-a.u. range for the helium and the molecular hydrogen target suggests that a similar ionization mechanism is operating for both targets. At large internuclear distances, a similarity in diabatic molecular orbital diagrams corresponding to the (He^+He) and the (He^+H_2) systems was already noted by Dowek *et al.* [48]. These authors and Jaecks *et al.* [50] observed many similarities between these systems in excitation and charge-exchange channels. Figure 3 shows that ionization in the intermediate velocity region occurs at larger τ for He than for H_2, a result that might result simply from the fact that there is no strong core potential from which the He^+ can scatter at small *b* for the molecular target. However, we note that for small *b*, where the rotational coupling presumably occurs, the degeneracy of the $2p\sigma$ and $2p\pi$ orbitals that occurs for He is more complex for H_2, for which the level energy curves must be replaced by energy surfaces and for which the shape of even these surfaces is dependent on the molecular alignment. It is therefore not obvious that the electron spectra, and thus presumably the ionization mechanisms, would be similar for these systems.

At the lowest projectile velocities (<0.5 a.u.) ionization paths of a different type, leading to the observed ''halo''-shaped electron distribution, seem to become more important for the He target. Evidence for the ''halo'' feature, which includes a large number of backscattered electrons, is present in Figs. 4(f), 4(g), 5(b), 5(e), and 5(f) and more weakly in Figs. 6(d)–6(f). It is strongest for soft, large-*b* collisions. This mechanism is also indicated by the shift toward smaller τ for the projectile velocity 0.25 a.u. in Fig. 3(b). We do not have a suggestion for the operative mechanism producing this feature.

At projectile velocities of 0.9 a.u. and above, there is also evidence for a different mechanism seen in the τ dependences of Fig. 3. We suspect that the shift toward smaller τ is indicative of the onset of a ''direct'' ionization mechanism, which is expected to occur as the projectile velocity approaches the target velocity. Such a mechanism shift from small-*b* molecular processes to large-*b* direct processes is predicted from the Massey criterion and is well known in many inelastic collision processes.

A detailed, quantitative comparison with calculations of these and other recent COLTRIMS data concerning ionization at low to intermediate impact velocity does not seem feasible at the present moment since the theoretical tools are still under development [41,51–54]. Calculations appearing in the literature in this range of V_P have been for the prototype *p* on H system only. The general character of these calculations have similarities to the data taken for more complex systems. The calculations of Macek and Ovchinnikov [41], carried out for proton impact on atomic hydrogen at energies of 5, 10, and 15 keV and at an impact parameter of 1.2 a.u., show that two broad, transverse concentrations appear in the in-plane electron momentum distributions, one located in the upper half ($P_{eY}>0$) and one in the lower half ($P_{eY}<0$) of the scattering plane. The maxima of these concentrations, arising from the *T* promotion mechanism (saddle-point mechanism) of the $2p\pi$ state, are situated

slightly off to the projectile beam axis, close to the middle point between target and projectile. A distinctive oscillation of the relative intensities of the two concentrations with impact velocity was noted, which reproduced the oscillatory behavior of the jetlike structures observed by Dörner *et al.* [37] in *p*-He collisions. From the data of Figs. 5–8 it is clear that not only π but also σ and δ amplitudes are present. The ability to account for the relative contributions of these amplitudes appears to be beyond the capability of any existing theoretical framework.

Sidky and Lin [54] used a discretization of the radial continuum to solve the Schrödinger equation in momentum space for proton impact at energies from 5 to 100 keV on atomic hydrogen and at an impact-parameter value of 1.2 a.u. Although no explicit mention of rotational coupling was made in the calculation, the results reproduced the two-fingered structure seen in the data of Figs. 5(c)–5(f) and Figs. 6–9 and in that of Dörner *et al.* [37]. This structure was identified within their formalism as being caused by a two-island structure: one island is associated with target projectile-centered basis states and one with target-centered states. The distribution of Fig. 9(d) for $V_P = 1.23$ a.u. especially bears a strong qualitative resemblance to their results. The oscillations seen by Macek and Ovchinnikov were not reproduced in this calculation. A more recent CTMC investigation of the role of the saddle-point promotion in these slow collisions by Sidky *et al.* [55] has suggested that only a small fraction of the continuum electrons released for 1 a.u. *p* on H originate from the saddle promotion scheme. This calculation is also able to reproduce a weak two-fingered structure in the distributions. The relationships among these very different theoretical approaches remains to be elucidated. Although all the theoretical results so far are for p on H, not the actual systems measured, we re-emphasize that there is remarkable similarity in the intermediate velocity range of the electron patterns for the collision systems (p, $He^{+,2+}$)-He and He^+-H_2. This similarity is taken as an indication that the molecular promotion mechanisms operative in all these collision systems are of a similar nature, and it therefore does not seem unreasonable to expect a similar mechanism for the *p*-H system.

V. CONCLUSIONS

By investigating the two collision systems He^+-He and He^+-H_2 over a larger range of projectile velocities, we were able to demonstrate that the appearance of geometric patterns in in-scattering-plane electron velocity distributions, currently interpreted as direct experimental evidence for the promotion of selected molecular orbitals into the continuum, are confined to a certain projectile velocity window that we have labeled a molecular promotion window. All measured data sets, such as reduced projectile scattering cross sections, side views and top views of electron velocity distributions, point toward the dominance, above about 0.45 a.u. impact velocity, of an ionization mechanism based on molecular promotion mediated by rotational coupling. This process begins to yield to a direct process at an impact velocity of above about 0.9 a.u. for He^+-H_2 and 1.23 a.u. for He^+-He. There is strong evidence that the molecular ionization mechanism is basically of the same nature for the two collision systems.

For velocities both above and below this window, different patterns, and presumably therefore different mechanisms, seem to enter for both targets. These processes are preferentially large-*b* ones. At low velocities the electron momenta lose the characteristic confinement to the collision plane. For the He target, the low-energy promotion mechanism produces ''halo'' electrons centered roughly on the target and extending well into the backward region. While it does not come as a surprise that at higher velocities the molecular promotion mechanism yields to a direct ionization process, the low-velocity behavior is much more puzzling. It might be argued that at low projectile velocities the rotational coupling becomes less effective, and ionization mechanisms of a different, and presently unknown nature, characterized by out-of-plane electron scattering, take over. The striking similarity of the main molecular promotion mechanism for ionization for the two targets is only partially understood. Only very qualitative arguments in favor of this similarity in the Discussion section can be given. We would like to stress the fact that the empirical data basis from which we can draw conclusions is still rather scanty, and investigations of additional collision systems, especially for a true one-electron system, would be of considerable importance.

ACKNOWLEDGMENTS

One of the authors (M.A.A.) gratefully acknowledges support received from the ORNL Program administrated jointly by the Oak Ridge Institute for Science and Education and the Oak Ridge National Laboratory. This work was supported by the Division of Chemical Sciences, Office of Basic Energy Sciences, Office of Energy Research, and U.S. Department of Energy.

[1] *Applied Atomic Collision Physics*, edited by H.S.W. Massey and D.R. Bates (Academic, New York, 1982).
[2] E.E. Nikitin and S.Ya. Unamskii, *Theory of Slow Atomic Collisions* (Springer, Berlin, 1984).
[3] U. Fano and W. Lichten, Phys. Rev. Lett. **14**, 627 (1965).
[4] W. Lichten, Phys. Rev. **164**, 131 (1967).
[5] J.C. Brenot, J. Pommier, D. Dhuicq, and M. Barat, J. Phys. B **8**, 448 (1975).
[6] J.C. Brenot, D. Dhuicq, J.P. Gauyacq, J. Pommier, V. Sidis, M. Barat, and E. Pollack, Phys. Rev. A **11**, 1245 (1975).
[7] M. Barat, D. Dhuicq, R. Francois, C.L. Lesech, and R. McCarroll, J. Phys. B **6**, 1206 (1973).
[8] G. Gerber, A. Niehaus, and B. Steffan, J. Phys. B **6**, 1836 (1973).
[9] M. Barat, D. Dhuicq, R. Francois, R. McCarroll, R.D. Piacentini, and A. Salin, J. Phys. B **5**, 1343 (1972).
[10] R. McCarroll and R.D. Piacentini, J. Phys. B **4**, 1026 (1971).
[11] V. Sidis, J. Phys. B **6**, 1188 (1973).

[12] W. Meckbach, P.J. Focke, A.R. Goni, S. Suarez, J. Macek, and M.G. Menendez, Phys. Rev. Lett. **57**, 1587 (1986).
[13] C.O. Reinhold and R.E. Olson, Phys. Rev. A **39**, 3861 (1989).
[14] G.C. Bernardi, S. Suarez, P.D. Fainstein, C.R. Garibotti, W. Meckbach, and P. Focke, Phys. Rev. A **40**, 6863 (1989).
[15] P.D. Fainstein, V.H. Ponce, and R.D. Rivarola, J. Phys. B **24**, 3091 (1991).
[16] Y.D. Wang, V.D. Rodriguez, C.D. Lin, C.L. Cocke, S. Kravis, M. Abdallah, and R. Dörner, Phys. Rev. A **53**, 3278 (1995).
[17] R.E. Olson, Phys. Rev. B **27**, 1871 (1983).
[18] R.E. Olson, Phys. Rev. A **33**, 4397 (1986).
[19] R.E. Olson, T.J. Gay, H.G. Berry, E.B. Hale, and V.D. Irby, Phys. Rev. Lett. **59**, 36 (1987).
[20] T.G. Winter and C.D. Lin, Phys. Rev. A **29**, 3071 (1984).
[21] W.L. Fite, R.F. Stebbings, D.G. Hummer, and R.T. Brackmann, Phys. Rev. **119**, 663 (1960).
[22] J.H. Macek and S.Yu. Ovchinnikov, Phys. Rev. A **50**, 468 (1994).
[23] S.Yu. Ovchinnikov and J.H. Macek, Phys. Rev. Lett. **75**, 2474 (1995).
[24] M. Pieksma and S.Yu. Ovchinnikov, J. Phys. B **25**, L373 (1992).
[25] M. Pieksma and S.Yu. Ovchinnikov, J. Phys. B **27**, 4573 (1994).
[26] E.A. Solov'ev, Phys. Rev. A **42**, 1331 (1990).
[27] A. Bárány and S.Yu. Ovchinnikov, Phys. Scr., T **46**, 243 (1993).
[28] M. Pieksma, S.Yu. Ovchinnikov, J. van Eck, W.B. Westerveld, and A. Niehaus, Phys. Rev. Lett. **73**, 46 (1994).
[29] V.D. Irby, T.J. Gay, J.Wm. Edwards, E.B. Hale, M.L. McKenzie, and R.E. Olson, Phys. Rev. A **37**, 3612 (1988).
[30] V.D. Irby, S. Datz, P.F. Dittner, N.L. Jones, H.F. Krause, and C.R. Vane, Phys. Rev. A **47**, 2957 (1993).
[31] T.J. Gay, M.W. Gealy, and M.E. Rudd, J. Phys. B **23**, L823 (1990).
[32] G. Bernardi, P. Fainstein, C.R. Garibotti, and S. Suarez, J. Phys. B **23**, L139 (1990).
[33] W. Meckbach, S. Suarez, P. Focke, and G. Bernardi, J. Phys. B **24**, 3763 (1991).
[34] R.D. DuBois, Phys. Rev. A **48**, 1123 (1993).
[35] S.D. Kravis, M.A. Abdallah, C.L. Cocke, C.D. Lin, M. Stöckli, B. Walch, Y.D. Wang, R.E. Olson, V.D. Rodriguez, W. Wu, M. Pieksma, and N. Watanabe, Phys. Rev. A **54**, 1394 (1996).
[36] M.A. Abdallah, S.D. Kravis, C.L. Cocke, Y. Wang, V.D. Rodriguez, and M. Stöckli, Phys. Rev. A **56**, 2000 (1997).
[37] R. Dörner, H. Khemliche, M.H. Prior, C.L. Cocke, J.A. Gary, R.E. Olson, V. Mergel, J. Ullrich, and H. Schmidt-Böcking, Phys. Rev. Lett. **77**, 4520 (1996).
[38] J. Ullrich, R. Dörner, V. Mergel, O. Jagutzki, L. Spielberger, and H. Schmidt-Böcking, Comments At. Mol. Phys. **30**, 285 (1994).
[39] R. Moshammer, M. Unverzagt, W. Schmitt, J. Ullrich, and H. Schmidt-Böcking, Nucl. Instrum. Methods Phys. Res. B **108**, 425 (1996).
[40] J.H. Macek, Nucl. Instrum. Methods Phys. Res. B **124**, 191 (1997).
[41] J.H. Macek and S.Yu. Ovchinnikov, Phys. Rev. Lett. **80**, 2298 (1998).
[42] M.A. Abdallah, C.L. Cocke, W. Wolff, H.E. Wolf, S.D. Kravis, M. Stöckli, and E. Kamber, Phys. Rev. Lett. **81**, 3627 (1998).
[43] M.A. Abdallah, W. Wolff, H.E. Wolf, C.L. Cocke, and M. Stöckli, Phys. Rev. A **58**, R3379 (1998).
[44] M.A. Abdallah, W. Wolff, H.E. Wolf, C.L. Cocke, and M. Stöckli, J. Phys. B: At. Mol. Opt. Phys (to be published).
[45] M. Stöckli, M.A. Abdallah, C.Y. Chen, C.L. Cocke, B.D. DePaola, D. Fry, P.E. Gibson, P. Richard, T.N. Tipping, B. Walch, S. Winecki, B. Eastman, Th. Gebel, E. Langer, U. Lehnert, H. Preusse, F. Ullmann, A. Gorges, and M. Rammasamy, Rev. Sci. Instrum. **69**, 665 (1998).
[46] A. Cassimi, S. Duponchel, X. Flechard, P. Jardin, P. Sortais, D. Hennecart, and R.E. Olson, Phys. Rev. Lett. **76**, 3679 (1996).
[47] M.A. Abdallah, C.L. Cocke, S. Kravis, E.C. Montenegro, R. Moshammer, L. Saleh, J. Ullrich, S.L. Varghese, W. Wolff, and H. Wolf, in *Application of Accelerators in Research and Industry*, edited by J.L. Duggan and I.L. Morgan (AIP, Woodbury, NY, 1997), p. 209.
[48] D. Dowek, D. Dhuicq, V. Sidis, and M. Barat, Phys. Rev. A **26**, 746 (1982).
[49] K. Taulbjerg, J.S. Briggs, and J. Vaaben, J. Phys. B **9**, 1357 (1976).
[50] D.H. Jaecks, O. Yenen, M. Natarajan, and D. Mueller, Phys. Rev. Lett. **50**, 825 (1983); C.L. Engelhardt and D.H. Jaecks, Phys. Rev. A **37**, 1041 (1988).
[51] S.Yu. Ovchinnikov, J.H. Macek, and D.B. Khrebtukov, Phys. Rev. A **56**, 2872 (1997).
[52] C. Harel, H. Jouin, B. Pons, L.F. Errea, L. Méndez, and A. Rieira, Phys. Rev. A **55**, 287 (1997).
[53] C. Illescas, I. Rabadán, and A. Riera, Phys. Rev. A **57**, 1809 (1998).
[54] E.Y. Sidky and C.D. Lin, Phys. Rev. A **60**, 377 (1999).
[55] E. Sidky, C. Illescas, and C.D. Lin (private communication).